

NUMERICAL INVESTIGATION OF THE ASYMPTOTIC BEHAVIOR OF TAPE SPRINGS

MICHELE COPPEDÈ, ROBERTO PARONI, MARCO PICCHI SCARDAONI

University of Pisa, Department of Civil and Industrial Engineering, Pisa, Italy

e-mail: m.coppede1@studenti.unipi.it; roberto.paroni@unipi.it; marco.picchiscardaoni@ing.unipi.it

Here, we investigate the behavior of the energy of a tape spring as its thickness becomes smaller and smaller. We consider the case of pure bending, i.e., we impose opposite rotations at both ends of the device. First, tape springs are introduced and their peculiar mechanical behavior is explained, and the details of the numerical model are carefully introduced. Then, a parametric study of the device is conducted for increasing end rotations and decreasing values of the thickness. Thus, we obtain parametric diagrams of reaction moments, energy per unit thickness, and energy densities. Finally, energy estimates are obtained.

Keywords: tape spring energy density, bending, elastic hinge, asymptotic behavior

1. Introduction

Tape springs are thin structures with transverse curvature (shells) used in many fields of engineering, for example in the aerospace engineering (CRTS reflector Seffen *et al.*, (2000)). These devices can be used as real deployment organs, thanks to their ability to form localized elastic hinges. This effect is entirely due to presence of the initial transverse curvature. An example of a daily use of these tapes is in carpenter's meters.

In their simplest form they are longitudinally straight, but they can also be provided with a non-zero initial longitudinal curvature. A fundamental characteristic common to all types of tape springs is the ability to concentrate the curvature even if there are no mechanical hinges, i.e., they are capable to form elastic hinges. The geometrical characteristics of straight tape spring devices are: length L , transverse radius of curvature R , angle subtended by the cross-section curve α and thickness t . The characteristics of an isotropic material are Young's modulus E and Poisson's ratio ν . The geometrical parameters are shown in Fig. 1. In general, the relation between the geometrical parameters can be summarized as follows: $t \ll a \ll L$, so these devices can be classified as shells.

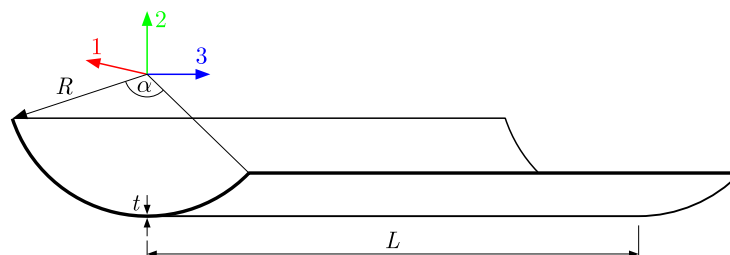


Fig. 1. Geometrical parameters of a straight tape spring

Many studies have been conducted on these devices in the past, mainly on the mechanical behavior under pure bending. In the work of Seffen and Pellegrino (1999), an introduction to the mechanical behavior of tape springs subjected to pure bending and an investigation about the

dynamic deployment of these devices is presented. In the article of Seffen *et al.* (2000), a study about curved tape springs is presented, showing that they have much in common with straight tape spring devices. A dissertation about the formation of elastic folds and an investigation of the mechanical behavior during pure bending is proposed in Seffen's PhD thesis (1997), where the author presents an estimate of key parameters of the moment-rotation relationship. A work about static and dynamic properties of three dimensional tape spring folds, using both experimental and theoretical methods, is presented in Walker's PhD thesis (2004). In the works of Guinot *et al.* (2012), Picault *et al.* (2013, 2014) and Martin *et al.* (2020) different beam models of tape springs are proposed in the case of pure bending, and in the one of Picault *et al.* (2016) there is an extension to 3D motions. In Kumar *et al.* (2023), the authors derive a one-dimensional model for tape springs that accounts for bending and twisting.

As shown in the literature, the moment-rotation relationship of tape spring devices undergoing pure bending is almost linear until a peak moment is reached, then it becomes highly non-linear as the elastic hinge forms. Due to this high non-linearity, the numerical modeling of these devices must be carefully addressed. A schematic example of the moment-rotation relationship is shown in Fig. 2.

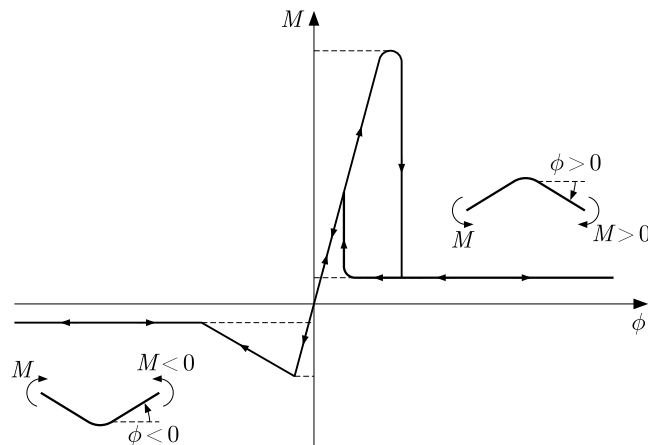


Fig. 2. Qualitative moment-rotation relationship, and lateral views of the deformed centerline in the post-critical regime (once the elastic hinge has taken place). For small rotations, the device deforms smoothly and follows a linear trend in the moment-rotation plane. When rotation increases, the behavior becomes highly non-linear and deeply different in the two cases of bending. This Figure is an adaptation of Fig. 2.4 of Walker's PhD thesis (2004)

It is observed that for small rotations the device deforms smoothly and follows a linear trend in the moment-rotation plane. When rotation increases, the behavior becomes highly non-linear and strongly dependent on the sign of rotation.

The purpose of this article is to highlight the behavior of tape springs as their thickness become smaller and smaller. The main novelty of this paper is to propose very simple formulas to obtain a good estimation of energy per unit thickness in the pre-critical and post-critical regime, in the case of pure bending.

2. Numerical model

Hereafter, we shall always refer to a straight cylindrical shell as shown in Fig. 1.

The characteristics of the examined specimen are those specified in Walker's PhD thesis (2004). The mechanical and geometrical parameters of the sample are: length $L = 267$ mm, cross section radius $R = 15.37$ mm, thickness $t = 0.1225$ mm, angle subtended by the cross section $\alpha = 1.719$ rad, Young's modulus 195300 MPa, Poisson's ratio 0.3.

The modeling and analysis challenges have been addressed with the Abaqus software (Smith, 2014).

The tape was simulated as a portion of a cylindrical surface, first modeling the cross section as a circumferential arc of radius R subtending an angle α .

In *Interaction* section two *Reference Points* located at the end cross sections were defined, then all the end nodes were constrained to the *Reference Point*, as shown in Fig. 3. The constraints were applied to the *Reference Points*. With reference to Fig. 1, the degrees of freedom constrained at the *Reference Point* at $x_3 = L$ are: translations in the three directions x_1 , x_2 and x_3 , rotations around the x_2 and x_3 axes. Instead, at the *Reference Point* at $x_3 = 0$, the degrees of freedom constrained are: translations in the directions x_1 and x_2 , rotations about x_2 and x_3 axes.

Rotations at the end cross sections are imposed: at the end $x_3 = 0$, rotation $\phi \mathbf{e}_1$ and at $x_3 = L$, rotation $\phi \mathbf{e}_1$, as shown in Fig. 3.

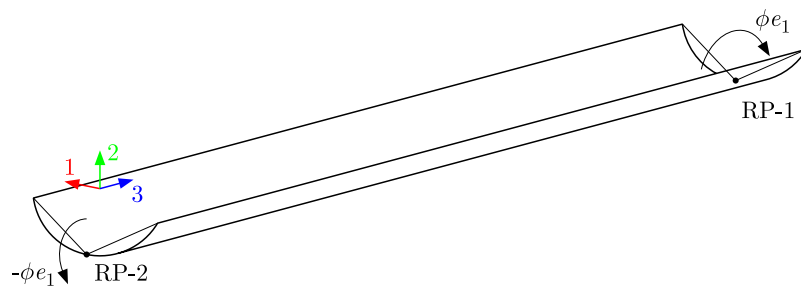


Fig. 3. Schematic view of the sample implemented in Abaqus. In this figure, there are reference points, RP-1 and RP-2 constrained, the segment from RP-1 and RP-2 represent constraints applied to the nodes of the end cross sections and the load condition

The size of the mesh was set up to 2.0 mm, for a total of about 1800 elements. *S8R5* elements were chosen, as in the works of Martin *et al.* (2020) and Picault *et al.* (2016), i.e., eight-node thin-shell elements with five degrees of freedom for each node with quadratic interpolation functions.

Static-Riks analysis was chosen, activating geometric non linearities and imposing the end of analysis when $\phi = \pi/2$. The settings of the step are: maximum number of increments 1000, initial arc length increment 0.01, minimum arc length increment 1E-10, the maximum arc length increment 1.2 and estimated total arc length 1.

The *arc length* method was originally developed by Riks (1972, 1979) and Wempner (1971). This approach is the most used *path following* method in the solution of non-trivial equilibrium paths. The Riks method solves simultaneously for both the load and displacements, and is the ideal method for solving problems of the tape spring devices, characterized by *snap-back* phenomena.

In Fig. 4, there is a view of the Abaqus model.

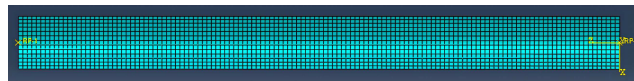


Fig. 4. Orthogonal projection of the Abaqus model on the x_1 - x_3 plane, visualized mesh

3. Main results

3.1. M - ϕ diagram

With reference to the characteristics of the tape specified in Section 2, eight different analyses were carried out, for opposite sense bending, varying thickness t of the device and keeping the

other geometrical and material parameters unchanged. The reference thicknesses are shown in Table 1.

Table 1. Thicknesses adopted in the analysis

Thickness t [mm]							
0.1215	0.1225	0.1300	0.1350	0.1400	0.1450	0.1500	0.1550

The thickness $t = 0.1215$ mm is the smallest thickness the convergence of analysis was achieved with.

We made sure that analysis results did not depend on the mesh size. The same analysis were carried out modifying the mesh, setting the mesh size to 1.0 mm for a total of about 3600 elements: the final results were the same.

Figure 5 shows the trends of the positive reactive moment as a function of rotation ϕ (Fig. 3), for the thickness values t shown in Table 1. Referring to the thickness $t = 0.1225$ mm, the results obtained here are in good agreement with those of Walker (2004), with an overestimation of the peak moment of about 7%. Instead, the stationary moment was quite close to the reference one.

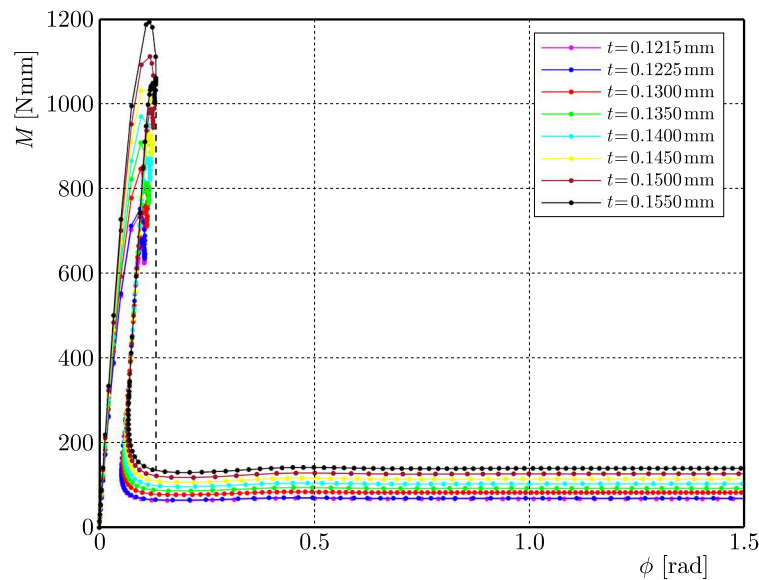


Fig. 5. M - ϕ diagram ($M > 0$)

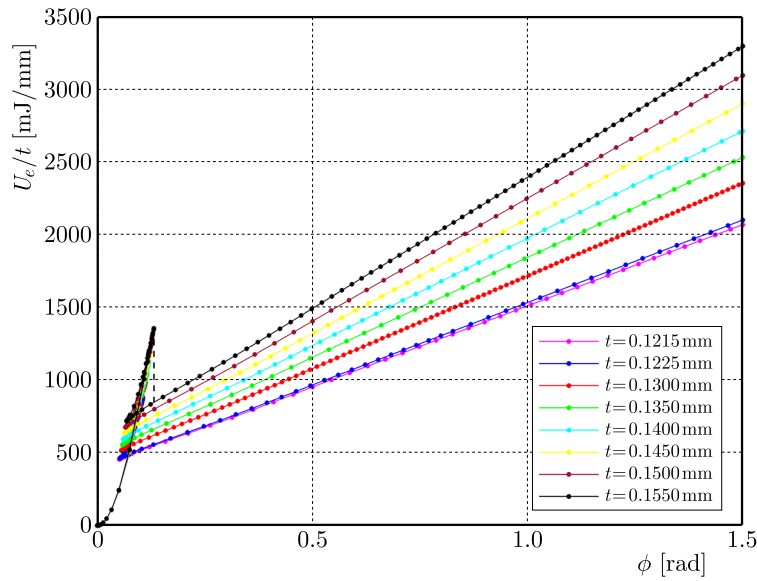
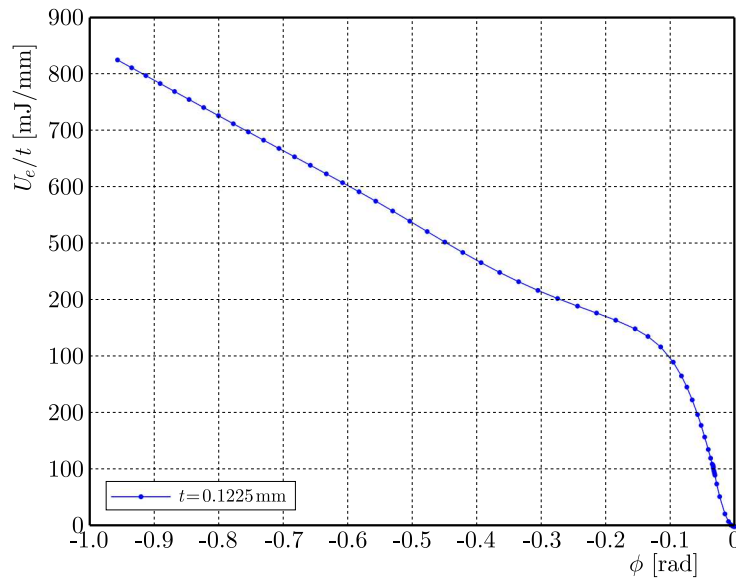
In Fig. 6, the energy per unit thickness versus rotation ϕ is represented, in the case of opposite sense bending, for the thickness values in Table 1.

From the M - ϕ diagram in Fig. 5, one can observe the typical trend described in previous works, for example Seffen and Pellegrino (1999), for these devices undergoing pure bending: the behavior is almost linear until the peak moment is reached, then the reactive moment M decreases and reaches a stationary value.

From Fig. 6, it can be seen that the trend is initially quadratic, corresponding to the linear behavior in the M - ϕ diagram, Fig. 5. In the post-critical regime, after formation of the elastic hinge, it is linear in ϕ .

For equal sense bending, various analyses were carried out relating to the same thicknesses used for positive bending. However, the convergence of the analysis in this case was much more difficult to achieve. We report just the case $t = 0.1225$ mm.

In Fig. 7, the energy per unit thickness versus the rotation ϕ in the case $t = 0.1225$ mm, for $M < 0$, is shown. Also, one can see that the energy trend is initially quadratic, then it is linear in ϕ .


 Fig. 6. U_e/t - ϕ diagram ($M > 0$)

 Fig. 7. U_e/t - ϕ diagram ($M < 0$)

To obtain the unloading path of the moment-rotation relationship, as in Fischer (1995), the command and change *restart analysis* was used decreasing the end rotation from $\phi = \pi/2$ to $\phi = 0$. The unloading paths found were the same as the loading ones.

For opposite and equal sense bending, the formation of the localized elastic hinge is due to buckling phenomena. We define the pre-critical regime when the device deforms prior to the elastic hinge has taken place, and post-critical regime when the device deforms after the formation of the localized elastic hinge.

Thanks to the analysis adopted, *Static-Riks* analysis, it is possible to detect *snap-back* phenomena that occur when, for opposite sense bending, the elastic hinge forms and there is a jump in the energy between the two stable solution branches. As shown in Fig. 6, for $t = 0.1550$ mm, the analysis captures the branch with a decreasing value of ϕ , but physically there is the *snap-back*, dashed line, that implies a jump in the energy between the two branches. In the same way

there is a jump, dashed line, in the reaction moment diagram $M-\phi$, as shown in Fig. 5, from the peak moment to the stationary one.

To estimate the transmission of potential energy distribution between the membrane and the flexural energy densities, which occurs right after the opening, it is enough to calculate the difference between the total energy before and after the formation of the localized elastic hinge.

3.2. Pre-critical regime

The pre-critical regime is before the formation of the localized elastic hinge.

As can be seen from the moment-rotation diagram for opposite sense bending, Fig. 5, for small values of ϕ , the moment is almost linear and the cross section varies its shape smoothly ("opening" of the cross section curve). Here, the energy has a quadratic trend, as represented in Fig. 6.

For the opposite sense bending, it is postulated that for small values of thicknesses t the energy per unit thickness can be represented by a formula of the following type

$$\frac{U_e}{t} = Ct^a\phi^b \quad (3.1)$$

In Eq. (3.1), C is some positive constant depending on the material and geometrical properties of the device, but not on the thickness.

To determine the exponents a and b , the energy per unit thickness is represented in a bi-logarithmic plane, in this way the exponents a and b are actually the slopes of the plotted curves, and the average slope of the curves can be determined. In the pre-critical regime, $a = 0$ and $b = 2$. The energy per unit thickness is independent of the thickness of the tape and quadratic in the rotation ϕ . Therefore, it is membranal regime, and the energy in Eq. (3.1) becomes

$$\frac{U_e}{t} = Ct^0\phi^2 \quad (3.2)$$

The diagrams of energy, normalized with respect to the thickness, are represented in Fig. 8.

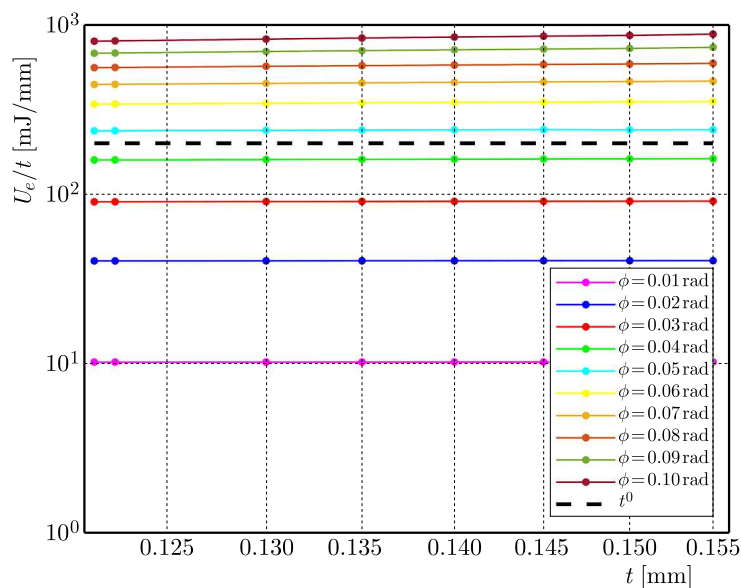
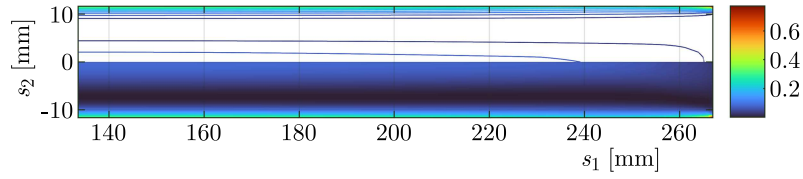
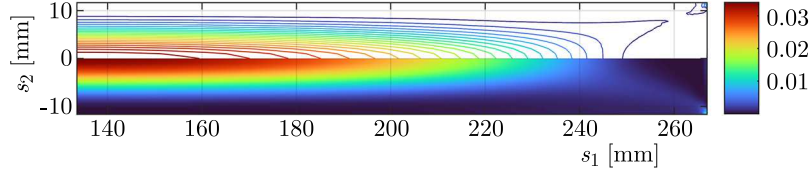
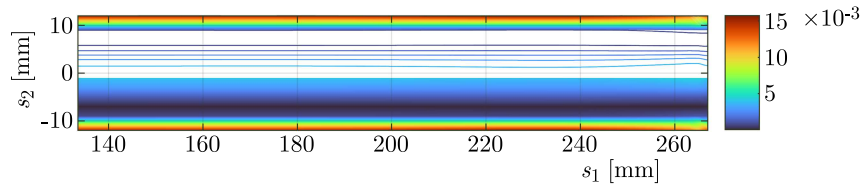
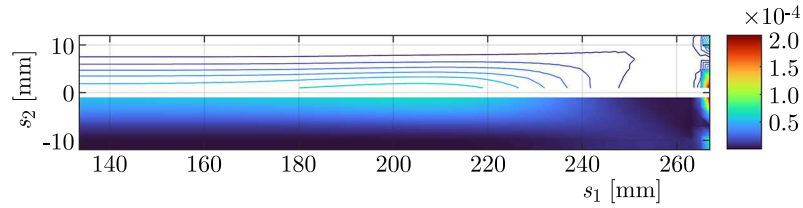


Fig. 8. $U_e/t-t$ diagrams in the pre-critical regime in a bi-logarithmic plane

To obtain the color maps of the energy densities of the shell model, the strain and the stress measures were exported, for every node, from Abaqus. Then, by post processing, we obtained


 Fig. 9. Membrane energy density u_m/t , pre-critical regime ($M > 0$)

 Fig. 10. Flexural energy density u_f/t , pre-critical regime ($M > 0$)

 Fig. 11. Membrane energy density u_m/t , pre-critical regime ($M < 0$).

 Fig. 12. Flexural energy density u_f/t , pre-critical regime ($M < 0$).

the energy densities by multiplying the membrane and bending strains by the energetically conjugate strains and changes of curvatures. The membrane and the flexural energy densities are represented in Figs. 9 to 12, for the opposite sense ($\phi = 0.1$ rad) and equal sense ($\phi = -0.1$ rad) bending, referring to $t = 0.1225$ mm. In these figures, s_1 represents the longitudinal abscissa of the shell, and s_2 the transversal one. Both the abscissas belong to the middle surface. It is observed that in the pre-critical regime the flexural energy density per unit thickness u_f/t is lower than the membrane energy density u_m/t , for both $M > 0$ and $M < 0$. Furthermore, the maps highlight a concentration of energy in the central area of the tape, close to the area where the elastic hinge will form.

3.3. Post-critical regime

During post-critical regime, i.e., in the case of well formed elastic hinge, the tape is characterized by another behavior in which the energy per unit thickness scales linearly with ϕ , Fig. 6.

For the opposite sense bending, it is postulated that for small values of thicknesses t the energy per unit thickness can be represented by a formula similar to the one used for the pre-critical regime

$$\frac{U_e}{t} = Ct^c \phi \quad (3.3)$$

Analogously, at the pre-critical regime, we got $c = 1.8$. Therefore, in the post-critical regime the normalized energy scales as $t^{1.8}$ and linearly in the rotation ϕ

$$\frac{U_e}{t} = Ct^{1.8}\phi \quad (3.4)$$

This means that in the post-critical regime there is a mixture of membranal and flexural energy, although the main component is flexural. The diagrams of the energy, normalized with respect to the thickness, are represented in Fig. 13.

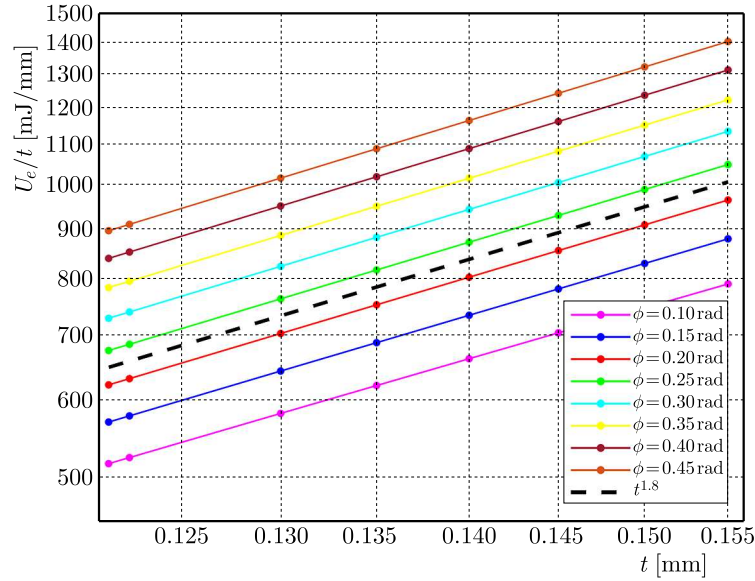


Fig. 13. U_e/t - t diagrams in the post-critical regime in a bi-logarithmic plane

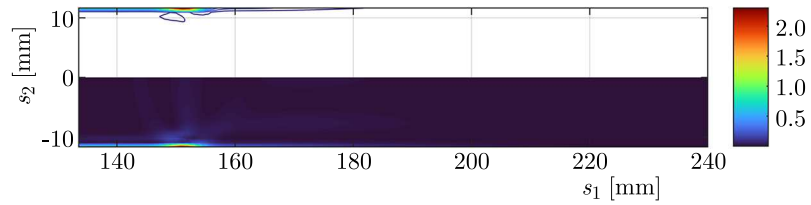
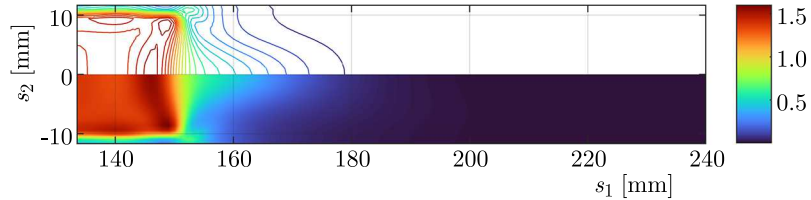
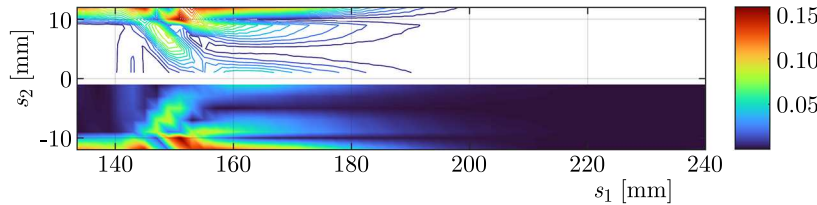
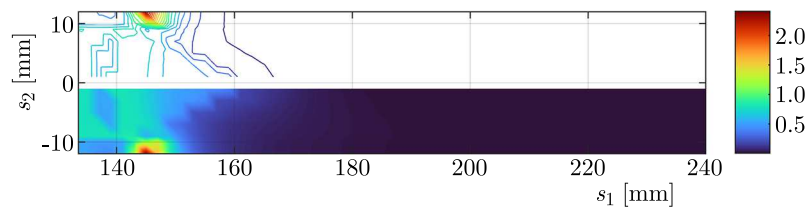
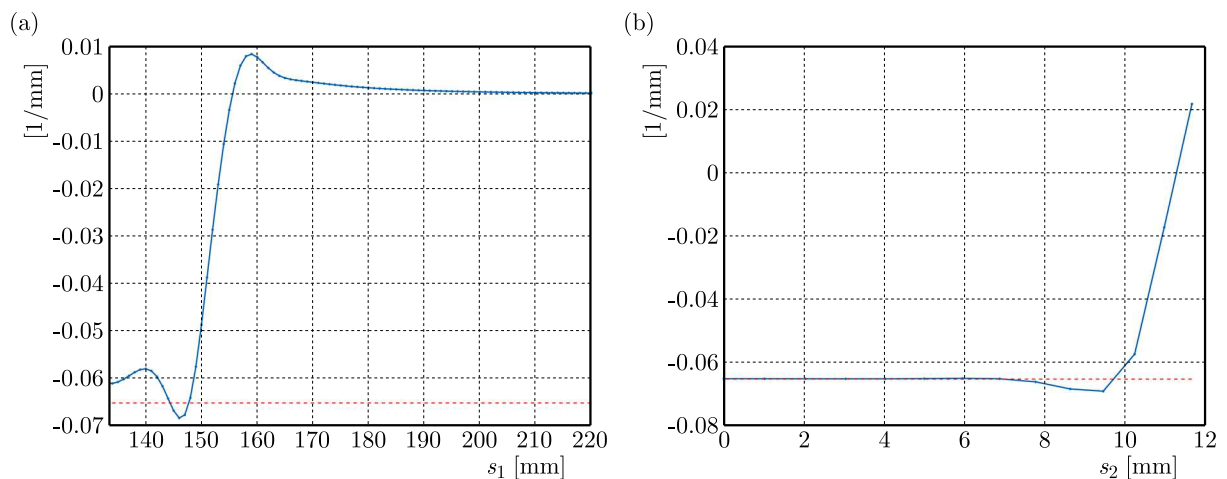
The membrane and flexural energy densities are represented in Figs. 14 to 17 for the opposite sense ($\phi = 1$ rad) and equal sense ($\phi = -1$ rad) bending, referring to $t = 0.1225$ mm. In these figures, s_1 represents the longitudinal abscissa of the shell, and s_2 the transversal one. In the post-critical regime for $M > 0$, it is observed that the membrane energy density per unit thickness u_m/t is approximately zero over the entire tape, with the exception of two areas near the hinge, where there is the transition from the almost constant curvature zone (hinge) and the transition zone. The energy u_f/t represents the largest contribution to the total energy density, and it is most concentrated in the hinge area where it is approximately constant.

Also in the case $M < 0$, the major contribution to the total energy density is given by u_f/t , however there are peaks near the hinge area.

In Figs. 18a and 18b, the trends of variations of longitudinal and transversal curvature are represented for $\phi = 1$ rad in the case $M > 0$.

From Fig. 18a, it can be seen that in the hinge area the longitudinal curvature is close to the initial transversal one, then the curvature increases very rapidly and after the maximum reached at $s_1 \approx 158$ mm becomes very close to zero, and is almost zero from $s_1 \approx 190$ mm. From Fig. 18b, it can be seen that most of the cross section has a constant curvature, while at the edges there is a residual curvature.

In the case $M < 0$, it is observed that the longitudinal curvature has a similar trend to the case $M > 0$. Also the trend of transverse curvature in the hinge area is similar to the case $M > 0$, with a concentration of curvature at the edges of the device.


 Fig. 14. Membrane energy density u_m/t , post-critical regime ($M > 0$)

 Fig. 15. Flexural energy density u_f/t , post-critical regime ($M > 0$)

 Fig. 16. Membrane energy density u_m/t , post-critical regime ($M < 0$)

 Fig. 17. Flexural energy density u_f/t , post-critical regime ($M < 0$)

 Fig. 18. On the left side, variation of the longitudinal curvature in the center of the tape (on a half of the tape length), on the right side, variation of transverse curvature in the hinge zone. In red dashed line, variation of the transversal curvature from the end configuration, perfectly flat, to the initial one. s_1 and s_2 are shell abscissas belonging to the middle surface. Figures (a) and (b) refer to post-critical regime ($M > 0$)

4. Conclusions

In this paper, a numerical analysis of a tape spring device is carried out. First, tape springs are introduced with a brief description of the particular mechanical behavior under pure bending. Then, the description of the numerical model is presented: mesh, type of mesh elements and the type of analysis conducted. Finally, the main results obtained are: moment-rotation diagrams for opposite sense bending (Fig. 5), energy diagrams per unit thickness for opposite sense and equal sense bending (Figs. 6 and 7), estimates of the energy per unit thickness Eq. (3.2) and Eq. (3.4), obtained from different analyses by varying the thickness of the device, and the color maps of the energies (Figs. 9-12 and 14-17). The moment-rotation diagrams obtained are typical of these devices, characterized by an almost linear trend for small rotations until a peak moment is reached. Then the reactive moment decreases and remains almost constant for further increments of rotation.

As regards the pre-critical regime, it was found that the energy expressed by Eq. (3.2) is typical of a membranal regime, i.e., the device deforms without activating the flexural regime.

For the post-critical regime, after formation of the localized elastic hinge, the energy expressed by Eq. (3.4) suggests the coexistence of the membrane and flexural regime, even if the major energy contribution is flexural.

Possible future developments could be: energy estimates for equal sense bending, development of beam models that are in agreement with these estimates for both opposite sense and equal sense bending.

Acknowledgement

This paper was presented at WECM'23 – 2nd Workshop on Experimental and Computational Mechanics (Pisa, Italy, 20-22 September 2023). Based on the evaluation by a Selection Committee chaired by Prof. Jerzy Warmański, Lublin University of Technology, Poland, and composed of Prof. Simone Camarri and Prof. Luigi Lazzeri, University of Pisa, Italy, this work was awarded the “WECM'23 Best Paper Award in Computational Mechanics”. The authors gratefully acknowledge the University of Pisa for organization of the workshop and for payment of the publication fee.

RP and MPS acknowledge the support from the University of Pisa through project PRA2022-69 “Advanced modeling of ultra-lightweight materials and structures”.

This work has been written within the activities of INdAM-GNFM.

References

1. FISCHER A., 1995. Bending instabilities of thin-walled transversely curved metallic strips, Report *cued/d-struct/tr 154*
2. GUINOT F., BOURGEOIS S., COCHELIN B., BLANCHARD L., 2012, A planar rod model with flexible thin-walled cross-sections. Application to the folding of tape springs, *International Journal of Solids and Structures*, **49**, 1, 73-86
3. KUMAR A., AUDOLY B., LESTRINGANT C., 2023, Asymptotic derivation of a higher-order one-dimensional model for tape springs, *Philosophical Transactions of the Royal Society A, Mathematical, Physical and Engineering Sciences*, **381**, 2244, 20220028
4. MARTIN M., BOURGEOIS S., COCHELIN B., GUINOT F., 2020, Planar folding of shallow tape springs: the rod model with flexible cross-section revisited as a regularized Ericksen bar model, *International Journal of Solids and Structures*, **188**, 189-209
5. PICAULT E., BOURGEOIS S., COCHELIN B., GUINOT F., 2013, Un modèle de poutre à section mince flexible pour l'étude du comportement 3d des mètres rubans, *Conference: 11e Colloque National en Calcul des Structures*, Giens, France

6. PICAULT E., BOURGEOIS S., COCHELIN B., GUINOT F., 2016, A rod model with thin-walled flexible cross-section: Extension to 3D motions and application to 3D foldings of tape springs, *International Journal of Solids and Structures*, **84**, 64-81
7. PICAULT E., MARONE-HITZ P., BOURGEOIS S., COCHELIN B., GUINOT F., 2014, A planar rod model with flexible cross-section for the folding and the dynamic deployment of tape springs. Improvements and comparisons with experiments, *International Journal of Solids and Structures*, **51**, 18, 3226-3238
8. RIKS E., 1972, The application of Newton's method to the problem of elastic stability, *Journal of Applied Mechanics*, **39**, 4, 1060-1065
9. RIKS E., 1979, An incremental approach to the solution of snapping and buckling problems, *International Journal of Solids and Structures*, **15**, 7, 529-551
10. SEFFEN K., 1997, *Analysis of Structures Deployed by Tape-Springs*, PhD Thesis, University of Cambridge
11. SEFFEN K., PELLEGRINO S., 1999, Deployment dynamics of tape springs, *Proceedings of the Royal Society of London. Series A: Mathematical, Physical and Engineering Sciences*, **455**, 1983, 1003-1048
12. SEFFEN K., YOU Z., PELLEGRINO S., 2000, Folding and deployment of curved tape springs, *International Journal of Mechanical Sciences*, **42**, 10, 2055-2073
13. SMITH M., 2014, Abaqus/standard users manual, version 6.14-5, Simulia, Providence, RI
14. WALKER S.J., 2004, *A Study of Three Dimensional Tape Spring Folds for Space Applications*, PhD Thesis, University of Southampton
15. WEMPNER G.A., 1971, Discrete approximations related to nonlinear theories of solids, *International Journal of Solids and Structures*, **7**, 11, 1581-1599

Manuscript received December 14, 2023; accepted for print February 20, 2024